Title Page

Title:

Activity and expression of carboxylesterases and arylacetamide deacetylase in human ocular tissues

Anam Hammid[1*], John K. Fallon[2], Toni Lassila[3], Paula Vieiro[4], Anusha Balla[1],

Francisco Gonzalez[5,6], Arto Urtti[1,7], Philip C. Smith[2], Ari Tolonen[3], Paavo Honkakoski[1*]

[1]School of Pharmacy, University of Eastern Finland, Yliopistonranta 1 C, 70210 Kuopio, Finland

[2]Division of Pharmacoengineering and Molecular Pharmaceutics, Eshelman School of Pharmacy, University of North Carolina at Chapel Hill, Campus Box 7355, Chapel Hill, North Carolina 27599-7355, United States

[3]Admescope Ltd, Typpitie 1, 90620 Oulu, Finland

[4]Biobank at the University Hospital at Santiago de Compostela (CHUS), 15706 Santiago de Compostela, Spain

[5]Center for Research in Molecular Medicine and Chronic Diseases (CIMUS), University of Santiago de Compostela, 15782 Santiago de Compostela, Spain

[6]Service of Ophthalmology, University Hospital of Santiago de Compostela, and Fundacion Instituto de Investigacion Sanitaria de Santiago de Compostela (FIDIS), 15706 Santiago de Compostela

[7]Faculty of Pharmacy, University of Helsinki, Viikinkaari 5 E, 00790 Helsinki, Finland

Running Title Page

Carboxylesterases in human eye tissues

Corresponding authors

Anam Hammid & Paavo Honkakoski

anam.hammid@uef.fi, paavo.honkakoski@uef.fi

School of Pharmacy, University of Eastern Finland

Yliopistonranta 1, Kuopio, FI 70211,

Tel. +358 465354577 (A.H.), +358403552490 (P.H.)

ORCID: 0000-0003-1939-7047 (A.H.), 0000-0002-4332-3577 (P.H.)

Number of text pages: 27

Number of Tables: 2

Number of Figures: 4

Number of references: 65

Word count in Abstract: 246

Word count in introduction: 747

Word count in discussion: 1488

Word count excluding references: 8078

Keywords: Human, ocular tissues, carboxylesterases, arylacetamide deacetylase, enzyme activity, proteomics

Abbreviations

AADAC, arylacetamide deacetylase; ACN, acetonitrile; ATP, adenosine triphosphate; BDNF, brain-derived neurotrophic factor; BSA, bovine serum albumin; CES, carboxylesterase; DPBS, Dulbecco's phosphate-buffered saline; DME, D-luciferin methyl ester; DMSO, dimethyl sulfoxide; DTT, dithiothreitol; FDA, fluorescein diacetate; LC, liquid chromatography; LLOQ, lower limit of quantitation; LLOD, lower limit of detection; MRM, multiple reaction monitoring; MS, mass spectrometry; NPA, 4-nitrophenol acetate; PABA, p-aminobenzoic acid; PBS, phosphate-buffered saline; RPE, retinal pigment epithelium; SIL, stable isotope-labeled; SPE, solid-phase extraction

Abstract

As a multi-tissue organ, the eye possesses unique anatomy and physiology including differential expression of drug-metabolizing enzymes. Several hydrolytic enzymes, that play a major role in drug metabolism and bioactivation of prodrugs, have been detected in ocular tissues but data on their quantitative expression is scarce. Also, many ophthalmic drugs are prone to hydrolysis. Metabolic characterization of individual ocular tissues is useful for the drug development process, and therefore, seven individual ocular tissues from human eyes were analyzed for the activity and expression of carboxylesterases (CESs) and arylacetamide deacetylase (AADAC). Generic and selective human esterase substrates 4-nitrophenyl acetate (most esterases), D-luciferin methyl ester (CES1), fluorescein diacetate and procaine (CES2), and phenacetin (AADAC) were applied to determine the enzymes' specific activities. Enzyme kinetics and inhibition studies were performed with isoform-selective inhibitors digitonin (CES1) and verapamil and diltiazem (CES2). Enzyme contents were determined using quantitative targeted proteomics, and CES2 expression was confirmed by Western blotting. The expression and activity of human CES1 among ocular tissues varied by >10-fold, with the highest levels found in the retina and iris-ciliary body. In contrast, human CES2 expression appeared lower and more similar between tissues whereas AADAC could not be detected. Inhibition studies showed that hydrolysis of fluorescein diacetate is also catalyzed by enzymes other than CES2. This study provides, for the first time, quantitative information on the tissue-dependent expression of human ocular esterases which can be useful for the development of ocular drugs, prodrugs, and in pharmacokinetic modeling of the eye.

Significance statement

Novel and comprehensive data on the protein expression and activities of carboxylesterases from individual human eye tissues are generated. In combination with previous reports on pre-clinical species, this study will improve the understanding of interspecies differences in ocular drug metabolism and aid the development of ocular pharmacokinetics models.

Introduction

The main route of drug clearance, hepatic metabolism, is extensively studied (Zhang and Tang, 2018; Li, 2021) whereas ocular drug metabolism is poorly understood (Dumouchel et al., 2018). The eye can be directly exposed by administered compounds; however, the role of local metabolism (del Amo et al., 2017; Dumouchel et al., 2018) is unclear although it may to some extent prevent accumulation of xenobiotics (Duvvuri et al., 2004). Therefore, estimation of activities and contents of ocular drug-metabolizing enzymes is important, not only for drugs administered systemically but also for topical and intravitreal drug delivery. Anatomical, physiological, and genetic differences between laboratory animals and humans complicate the translation of animal metabolic data to humans (Argikar et al., 2017; del Amo et al., 2017). A well-studied metabolic profile of the human eye and comparisons to preclinical species would significantly benefit ocular drug development.

Recent studies have indicated that various functionalization (cytochrome P450s, dehydrogenases, reductases, esterases and peptidases) and conjugation enzymes (acetyl-, glucuronosyl-, glutathione and sulfotransferases) are present at the activity, mRNA and/or protein levels in some rat, rabbit, pig, human, and bovine ocular tissues (reviewed by Al-Ghananeem and Crooks, 2007; Argikar et al., 2017; Ahmad et al., 2018; Dumouchel et al., 2018). The metabolism of ketoconazole (Cirello et al., 2017), levobunolol (Argikar et al., 2016), and betaxolol (Bushee et al., 2015) has been observed in whole eye S9 fractions from rats, rabbits, and humans, indicating the intrinsic metabolic capacity of the eye.

Bioactivation of ester prodrugs is well documented in laboratory animals. Ester prodrugs of e.g. epinephrine (Mandell et al., 1978; Nakamura et al., 1993), ganciclovir (Macha et al., 2004), latanoprost (Sjöquist et al., 1998; Xiang et al., 2009), timolol (Volotinen et al., 2011)

and pilocarpine (Saarinen-Savolainen et al., 1996) are hydrolyzed to active drugs. Moreover, ocular tissues display variable esterase-mediated activities: hydrolysis of pilocarpine to pilocarpic acid occurs in the iris-ciliary body, retina, and choroid (Ellis et al., 1972), and bimatoprost free acid is formed in the rabbit and human cornea, sclera, and iris-ciliary body (Davies et al., 2003; Hellberg et al., 2003). We found that hydrolysis of cefuroxime axetil was high in the rabbit cornea, aqueous humor, and iris-ciliary body (del Amo et al., 2022).

With probe substrates, a significant hydrolysis of naphthyl esters has been detected in rabbit iris-ciliary body, cornea, and aqueous humor (Lee et al., 1982, 1983; Lee, 1983). Similarly, the highest rates of NPA hydrolysis are observed in rabbit cornea and iris-ciliary body (Heikkinen et al., 2018). We published recently, for the first time, significant species and tissue differences in protein expression and activities of esterases (Hammid et al., 2021). Carboxylesterase 1 (CES1) were observed in both rabbit and pig, CES2 was found only in rabbits, while CES3 and arylacetamide deacetylase (AADAC) were not detected. The CES1 contents and associated activities showed up to 10-fold differences, with retina and iris-ciliary body being the highest and conjunctiva and cornea the lowest (Hammid et al., 2021).

Due to the limited tissue availability, data on human ocular metabolic enzymes originates mostly from human cultured cells or whole eye homogenates (Argikar et al., 2017). Thus, the tissue-specific expression of various esterases is vastly understudied (Attar et al., 2005; Dumouchel et al., 2018). As far as we know, the hydrolytic activities of human ocular tissues using a probe substrate have not been determined comprehensively. However, CES isoforms and other hydrolases have been identified in most human tissues using post-mortem homogenates and different proteomic techniques (Ahmad et al., 2018). Specifically, CES1 has been detected in the cornea (Galiacy et al., 2011), lens (Hains and Truscott, 2010), vitreous (Skeie et al., 2015), retina, and iris-ciliary body (Zhang et al., 2015, 2016), and

RPE/choroid (Skeie and Mahajan, 2014). In contrast, a recent study identified only CES4/CES1P1 among CES isoforms in S9 fractions of pooled human eye homogenates (Balhara et al., 2021). Such qualitative data cannot fully estimate the metabolic profile of human eye tissues.

To address this gap, we have measured the activities and absolute quantities of main CES isoforms and AADAC in seven human ocular tissues obtained from post-mortem or surgical samples. The enzyme activities were determined by general and isoform-selective probe substrates while the protein contents were analyzed using targeted proteomics with isotope-labeled standard peptides. Inhibition studies were conducted to validate the specificity of enzyme substrates. Here, CES1 seems to be active and present in multiple human eye tissues whereas the CES2 enzyme is expressed at lower levels. We did not find any substantial AADAC activity or protein expression.

Materials and Methods

Chemical and reagents.

Hydrolysis assays. Acetaminophen, acetonitrile (ACN), Bio-Rad protein assay dye reagent (# 500-0006), BSA, dimethyl sulfoxide (DMSO; $\geq$ 99.9 %), D-luciferin, fluorescein diacetate (FDA), fluorescein, 4-nitrophenyl acetate (NPA), 4-nitrophenol, *p*-aminobenzoic acid (PABA), phenacetin, p-phenetidine ($\geq$ 99.9 %), procainamide-HCl ($\geq$ 98 %), phosphate-buffered saline (PBS), and procaine-HCl (> 97 %) were from Sigma-Aldrich Finland Oy (Espoo, Finland). D-luciferin methyl ester (DME) was produced by AAT bio-quest (Sunnyvale, CA, USA) while rLuciferase (QuantiLum® recombinant luciferase) was purchased from the Promega (Madison, WI, USA). Thermofisher Scientific (Massachusetts, USA) provided the 10 × DPBS stock (# 14200166). All purchased compounds were of analytical grade. Chemicals and reagents.

Targeted proteomics. Ammonium hydrocarbonate, ACN (MS grade), chloroform, dithiothreitol (DTT), formic acid, guanidine hydrochloride, iodoacetamide, methanol, sodium hydroxide sodium-EDTA, and Trizma® (Tris base) were products of Sigma (Saint Louis, MO, USA). Customized stable isotope labeled (SIL) peptides (SpikeTides^{TM}_TQL) were purchased from JPT Peptide Technologies GmbH (Berlin, Germany). TPCK-treated trypsin, ProteaseMAX, sequencing-grade lysyl endopeptidase, and urea were products of Promega (Madison, WI, USA) while 10 mg/mL cartridges (33 μm, polymeric reversed-phase [Part # 8B-S100-AAK]) used for solid-phase extraction (SPE) were from Phenomenex (Torrance, CA, USA).

Sample collection. Human eyes were provided by the biobank at the University Hospital at Santiago de Compostela, Spain. All tissue samples used in this study were obtained either

from post-mortem donors or from patients who required eye evisceration. Patients and donors were of Caucasian ethnicity and their characteristics are listed in Supp. Table 1 and 2. All procedures followed the tenets of the Declaration of Helsinki and were authorized by the Comite de Etica de la Investigacion de Santiago-Lugo, Spain. All dissection procedures were carried out under aseptic conditions at the University Hospital Complex of Santiago de Compostela, Spain, and all samples were stored at the biobank of the same institution. The transfer of authority to use human ocular tissues was done under the research project entitled "Educational Network in Ocular Drug Delivery and Therapeutics" (Ethics approval code 42/2014). The rat whole eye pool (covered by the license # ESAVI/8621/04.10.07/2017) and the single human liver sample (donated by Prof. Olavi Pelkonen, from Oulu University Hospital) were simply included solely as positive control samples for the assays as described earlier (Hammid et al., 2021). They should not be used to compare between the hepatic and ocular tissue activities and protein contents which would require multiple human liver donors.

Eye globes were collected from post-mortem male (10) and female (4) donors, aged 52 – 83 years (Supp. Table 1). Samples were obtained between two and four hours post-mortem. In most cases, the cornea was removed before enucleation for transplant purposes. Conjunctival samples were taken from the four quadrants of the bulbar conjunctiva. Then the eyes were enucleated, and the vitreous content was saved. For this, the eyelids were retracted with a lid speculum, and each extraocular muscle was isolated and cut at its insertion on the sclera. Finally, the optic nerve was cut, the whole eye removed, placed on ice, and subsequently stored at -80 ºC.

Corneas were collected from male (3) and female (6) patients, aged 16 – 88 years, who required evisceration (Supp. Table 2). For this, the sclera was cut 360 degrees around the

surgical limbus. Then the eye lens was removed and the vitreous and the retina were carefully extracted, placed in a small polypropylene tube on ice, and subsequently stored at -80 ºC.

Tissue homogenate preparation. The tissues were extracted and homogenized according to our published protocol (Hammid et al., 2021). Briefly, the frozen eye globes without corneas from the donors were thawed on ice, conjunctival tissues were collected first, followed by the collection of the lens, iris-ciliary body, vitreous, and retina. Corneal samples of the patients were combined.

During tissue dissection, care was taken to minimize tissue cross-contamination. The relatively firm anterior tissues (conjunctiva, cornea, lens, and iris-ciliary body) were cleanly separated from each other while still in frozen state. The softer posterior tissues (vitreous, retina, RPE/choroid) are adjacent to each other and required more attention in preparation. Only the colorless parts of the vitreous were collected, the retina detached cleanly from the RPE as a single layer, and the choroid and sclera were also well separated from each other. Because it was impossible to fully separate pure RPE and choroid tissues from the frozen eyes, RPE was collected by scraping into Dulbecco's phosphate-buffered saline (1 × DPBS) and combined with the choroid sample (hereafter called RPE/choroid). We noted that it was not possible to obtain 100% purity among soft posterior tissues and evaluated potential contamination using antibodies to retina- and RPE-specific proteins, brain-derived neurotropic factor (BDNF), (Mowla et al., 2001) and bestrophin-1 (Marmorstein et al., 2000), respectively.

For each tissue, four samples from different individuals were randomly combined to make one pool, and three separate pools from each tissue were used for the experiments. Pooling was necessary to obtain sufficient material for enzymatic assays.

Tissue pool were homogenized in 1 × DPBS buffer (3:1, volume/tissue weight) with a Bead Ruptor Elite homogenizer using 2.8 mm ceramic beads by Omni Internationals (Kennesaw, GA, USA) using two 4-min cycles at a speed of 6 m/s as described earlier (Balla et al., 2021). Supernatants of tissue pool homogenates were collected after brief centrifugation (5 min at 10,000 g), aliquoted, and stored at -80 °C. Bio-Rad assay (Bradford, 1976) was used to quantify the protein contents in samples. Bovine serum albumin (BSA) (0.25 – 2 mg/ml) was used as the standard.

Hydrolytic enzyme assays

Hydrolysis of 4-nitrophenol acetate (NPA). The hydrolysis of NPA in ocular tissues was assessed using the previously published protocol for the preclinical species (Hammid et al., 2021). Briefly, the changes in absorbance due to the hydrolysis of NPA to 4-nitrophenol were measured using 96-well clear bottom flat plates (Thermo Scientific™ Sterilin™ Microtiter™). The 8-µg protein samples (diluted in PBS) were pre-incubated for 10 min at 37°C and the background readings were measured. The reaction was started by adding substrate (final concentration 400 µM) into the wells. The absorbances at 405 nm were recorded for 45 min with 90-s intervals using a Victor[2] Microplate Reader (PerkinElmer, St. Paul, MN, USA). Stock solutions of 4-nitrophenol (5 – 400 µM) were used to generate the standard curve.

Hydrolysis of D-luciferin methyl ester (DME). Hydrolysis of DME (Hou et al., 2016) was monitored using our optimized protocol for ocular samples (Hammid et al., 2021). In a white-coated 96-well plate (Thermo Scientific), 5-µg protein samples diluted in 0.1 M PBS, pH 6.5 were incubated for 20 min at 37°C together with DME (5 µM) to generate the product D-luciferin. D-luciferin was quantified by injection of 73 µL detection reagent [3 µg rLuciferase, 0.4 mM of ATP, and 0.7 mM of $MgCl_2$ in PBS] into the wells, and luminescence

12

was recorded with a Victor^2 Microplate Reader. The standard curve of D-luciferin (0.156 – 10 µM) was generated in 0.1 M PBS, pH 6.5.

Hydrolysis of fluorescein diacetate (FDA). The hydrolysis of FDA to fluorescein (Wang et al., 2011) was measured using a fluorometric assay as described previously (Hammid et al., 2021). The 5-µg protein samples in PBS (0.1 M, pH 7.4) were preincubated for 5 min at 37 °C in black-coated 96-well plates (Nunc™ F96 MicroWell™, Thermo Scientific). Initially, background fluorescence was measured at the excitation and emission wavelengths of 485 nm and 535 nm, respectively, with a Victor^2 Microplate Reader. FDA (100 µM) was then added to each well to start the reaction. Fluorescence measurements were taken over 30 min with a 60-s interval between each reading. A standard curve (0.156 – 10 µM) was generated using two-fold serial dilutions of fluorescein stock solution in 0.1 M PBS, pH 7.4.

These assays were conducted under optimized conditions, where the activities were linearly dependent on protein concentration and incubation time. The organic solvent content in samples was kept below 0.5% (v/v). The standard curves were used to calculate the specific activities. Two blanks, either by replacing the enzyme source or the substrate with buffer, were used in each assay to subtract the non-specific hydrolysis from the samples' specific activities. All the assays were performed using three pools of tissues and three technical replicates to calculate the average mean and ± standard deviation (SD).

Determination of kinetic parameters. Among the human ocular tissues, the retina and iris-ciliary body showed the highest hydrolytic activities. These tissues were used to determine the Michaelis-Menten constant (K_m) and maximum reaction velocity (V_{max}) of NPA, FDA, and DME hydrolysis. The increasing substrate concentrations (seven per assay; 37.5 – 2000 µM for NPA, 0.3 – 20 µM for DME, and 3.12 – 200 µM for FDA) were incubated with the protein content of 5-8 µg in triplicate as described in the earlier study (Hammid et al., 2021).

13

Inhibition studies. Human RPE/choroid, iris-ciliary body, and retinal tissues displayed the highest hydrolysis rates for DME and FDA and hence used for the inhibition studies. Increasing final concentrations of digitonin, a known CES1 inhibitor (Shimizu et al., 2014), and verapamil diltiazem and timolol, both known CES2 inhibitors (Zou et al., 2017), were used from 0.13 to 200 µM. The substrate concentrations near the K_m values for DME (5 µM) and FDA (30 µM) were adopted. The inhibitors were replaced by the DMSO solvent in the blank reactions.

LC-MS analysis of procaine and phenacetin hydrolysis

Procaine hydrolysis. The CES2 substrate procaine (Jewell et al., 2007) was incubated with human ocular tissue homogenates according to a previously published protocol (Dhananjeyan et al., 2007). The substrate solution (100 µM procaine in 0.1 M Tris-HCl buffer, pH 7.4) was preincubated for 5 min at 37 °C. Sample (20 µg protein) was added to initiate the hydrolysis in a total reaction volume of 200 µL. The reaction mixtures and the two blank samples (no enzyme, no substrate) were placed on the shaker incubator (Heidolph Titramax 1000 platform shaker, Berlin Germany). After 50 min of incubation at 37 ⁰C, the reaction was terminated using an equal volume of ice-cold ACN containing 1 µM internal standard procainamide. The reaction mixture was centrifuged at 4⁰C for 10 min at 10,000 *g* and the supernatants were collected for HPLC analysis. The hydrolysis product (PABA; 10 nM to 1000 nM) was used to establish the standard curve (Dhananjeyan et al., 2007).

Phenacetin hydrolysis. The arylacetamide deacetylase (AADAC) substrate phenacetin was incubated with human ocular homogenates (Kudo et al., 2000; Watanabe et al., 2010). First, the substrate (4 mM) was preincubated in 0.1 M Tris-HCl buffer, pH 7.4 for 5 min at 37 ⁰C. This was followed by the addition of the sample (20 µg protein) to initiate the reaction that was further incubated for 50 min at 37 ⁰C. The reaction was stopped with an equal volume of

14

ice-cold ACN which contained 1 µM acetaminophen as the internal standard. For the LC-MS analysis, the supernatant was collected, and a standard curve was established with p-phenetidine stock solutions of 0.0312 – 20 µM.

The experimental conditions for both procaine and phenacetin were optimized in the pilot experiments to ensure linearity with protein concentration and incubation time. All the assays were performed in triplicate and the mean ± SD was calculated.

Metabolite quantification using LC/Q Orbitrap MS. The samples were subjected to ultra-performance liquid chromatographic analysis (UPLC) with the Acquity system (Waters, Milford, MA, USA), equipped with Orbitrap MS (Thermo Scientific™) as described earlier (Lassila et al., 2015). The elution column was HSS T3 (particle size 1.8 µm 2.1×100 mm, Waters), The mobile phases A (0.1 % formic acid) and B (methanol) were employed for the following elution gradients: 1% B at 0 – 0.5 min, 1 – 20% B at 0.5 – 4 min, 20-98% B at 4 – 4.5 min, 98% B at 4.5 – 5 min and 98 – 1% B at 5 – 6 min. The injection volume was 2 µL with a flow rate of 0.5 mL/min. A positive ionization mode with the mass range of 70 – 1000 m/z was acquired. To process the data, an external calibrator system was adopted using Thermo Xcalibur by Thermo Fisher Scientific (version 4.1.31.9). The lower limit of quantification (LLOQ) for procaine and phenacetin hydrolysis was 0.02 and 0.06 pmol/min/mg protein, respectively.

Quantitative targeted proteomics analysis

Stable isotope-labeled (SIL) peptides. Quantification of CES1, CES2, and AADAC enzymes in human ocular tissues was performed using proteotypic peptides (Table 1). Peptides were designed to cover conserved protein sequences between species and were already verified in our previous study (Hammid et al., 2021).

Sample preparation. Proteomics samples were prepared following the previously established quantitative targeted protocols (Uchida et al., 2013). Protein samples (100 μg) were denatured by adding a solubilizer mixture (7 M guanidine hydrochloride, 3 M Tris-HCl pH 8.5, and 0.5 M Na_2-EDTA pH 8.0, final volume 220 μL) followed by the addition of DTT (100 μg) and iodoacetamide (250 μg) at room temperature in the dark. The S-alkylated proteins were precipitated by the addition of ice-cold methanol (600 μL), chloroform (150 μL), and deionized water (450 µl). Tubes were mixed thoroughly and centrifuged at +4 ⁰C for 5 min at 15,000 *g*. The lipid layer was discarded, and the pellet was washed with 450 µl of ice-cold methanol. The pellet was resuspended in 6 M urea (9 µL) and 0.1 M Tris-HCl pH 8.5 (36.5 µL) and sonicated to resuspend it completely (30-sec cycles: Sonorex Super RK 102 H, Berlin, Germany). SIL peptides (1.5 fmol of each peptide/μg protein) from a mixture were added and digestion was started by adding LysC (0.5 μg) and proteaseMax (final concentration 0.05 %) to the sample tubes. After three hours, TPCK-treated trypsin (0.5 μg) was added, and the mixtures were incubated overnight at 37 °C. The reactions were stopped with 3 μL 20% formic acid, centrifuged at 15,000 *g* at +4 °C and the supernatants were collected into clean vials. Each sample (20 μg of digest) was processed by SPE before being analyzed by nanoLC−MS/MS as described in the next section.

For SPE, cartridges (C18, 10 mg/mL) were conditioned with methanol and deionized water (250 μL of each). Digested samples were applied, and cartridges were washed with deionized water (150 μL). Peptides were eluted into protein low binding tubes (0.5 mL LoBind; Eppendorf, Enfield, CT, USA) with 250 μL of 0.1% formic acid and ACN (40:60, v/v). The eluants were dried and reconstituted in 2% ACN (50 μL) and centrifuged for 5 min at 13,400 *g*. Supernatants were transferred into deactivated vial inserts for analysis**.**

16

NanoLC-MS/MS analysis. The details of the analysis were reported in our previous publications (Khatri et al., 2019; Hammid et al., 2021). Briefly, the nanoLC-MS/MS system consists of a nanoAcquity (Waters) coupled to a QTRAP 5500 with a NanoSpray III source (SCIEX, Framingham, MA). The mobile phase A was 1% ACN and 0.1% formic acid in deionized water and B was 100% ACN. The injected volume was 0.2 µL which corresponded to 0.08 µg of the sample or 0.4% of the nominal sample amount (20 µg). The trap column was a Symmetry C18 (Waters, part # 186006527, 5 µm particle size, 180 µm × 20 mm). The trapping flow was 15 µL/min of mobile phase A for 1 min. The analytical column was 150 mm × 100 mm Waters, part # 186003550. The flow rate was 1.3 µL/min, and the gradient method was as follows; eluent A, 100 % at start decreasing to 58 % at 24 min, decreasing to 5 % at 24.5 min for three min and increasing to 100 % between 27.5 and 28 min. This was held for equilibration until 35 min, which was the total run time. The mass spectrometer was operated in the positive mode. The ion spray voltage was set at 4000 V. For each peptide, a 90 sec scheduled acquisition window was used.

Multiple reaction monitoring (MRM) was the mass spectrometer data acquisition method used. For the SIL peptide standards, a range of transitions was predicted by Skyline software (version 2.6, University of Washington). After initial injection of the standards onto the system, five transitions with the highest response for each peptide were selected. Collision energies for these transitions were optimized by repeated injection onto the system without changing declustering potentials. Two MRMs with the best response were chosen for the concentration calculations. MultiQuant 2.0.2 (SCIEX) was used to process the MRM data (Supp. Table 3).

To calculate the peptide concentrations, the area ratio of unlabeled to the known amount of SIL peptides was used (0.15 pmol of each SIL peptide had been added to the initial 100 µg

17

protein sample). The responses of SIL and unlabeled peptides were assumed equal. The peptide with the highest values was used to report the concentration of proteins while a second peptide, if available, was used for confirmation.

Western blotting

Protein samples (40 μg) from ocular tissues and positive control homogenates, along with the molecular marker ladder (10–250 kDa, Precision Plus Protein™ Dual Color, Bio-Rad, CA, USA) were loaded on the wells of commercially available SDS−PAGE gels (4−20% Mini-PROTEAN TGX precast gels, Bio-Rad). Electrophoresis was performed for 1 hour at 180 V until the dye reached the bottom of the gel.

Proteins were then transferred onto a PVDF membrane (Bio-Rad) by adopting semidry electroblotting (60 min, 15 V, 300 mA; Trans-Blot SD, Bio-Rad) followed by one-hour incubation at room temperature in blocking solution (3 % milk powder and 0.1 % Tween 20 in PBS) and washing of the membrane thrice with 0.1% Tween 20 in PBS. This was followed by the incubation with the primary antibody (rabbit-anti CES2 1:1000, #PA5-102415, ThermoFisher Scientific, Waltham, MA, USA) overnight at +4 °C.

Secondary antibody incubation (goat anti-rabbit, sc-2030, 1:10000; Santa Cruz Biotechnology, Santa Cruz, CA, USA) was conducted at room temperature for 45 min, followed by washing with 0.1% Tween 20 in PBS three times. Finally, to detect the protein−antibody complexes, SuperSignal™ West Femto Western Blotting Detection Reagent (Thermo Scientific) was used according to the manufacturer's instructions with a chemiluminescence reaction (Image Quant RT ECL, GE Healthcare, Little Chalfont, U.K.).

Tissue cross-contamination between the posterior samples (vitreous, retina and RPE/choroid) were analyzed by Western blotting but using 20 μg protein per lane and antibodies to the

18

retina marker (rabbit anti-BDNF, dilution 1:1000; #AB1534SP, EMD Millipore, CA, USA) and RPE marker (mouse anti-bestrophin, dilution 1:1000; #NB300-164, Novus Biologicals, Toronto, Canada). Respective secondary antibodies (goat anti-rabbit IgG, sc-2030, and goat anti-mouse IgG, sc-2005 at 1:10000 dilution; both from Santa Cruz Biotechnology, Santa Cruz, CA, USA) were used to visualize the proteins as described above.

Statistical analysis

ANOVA followed by the Mann-Whitney U test (Sigma Plot 13.0, Systat Software Inc., San Jose, CA, USA) were applied to compare between eye tissues. Statistically significant differences in enzyme activities or amounts are denoted as follows: *, $p < 0.05$; **, $p < 0.01$ and ***, $p < 0.001$. Furthermore, for the calculation of kinetic parameters, K_m and $V_{max,}$ non-linear regression analysis was done using GraphPad Prism (GraphPad Prism 5.04; Software Inc., San Diego, CA).

Results

Hydrolysis of NPA, DME, and FDA substrates

The hydrolytic activities of ocular tissues towards NPA, DME, and FDA substrates are presented in Figure 1A-1C. Among human ocular tissues, iris-ciliary and vitreous displayed the highest rates of NPA hydrolysis of 81 ± 34 and 75 ± 22 nmol/min/mg, respectively Figure 1A. Human conjunctiva, retina, cornea, and RPE/choroid had similar hydrolysis rates from 17 ± 1.8 to 23 ± 7.5 nmol/min/mg while the activity in the lens was the lowest at 4 ± 1 nmol/min/mg. Overall, the hydrolysis rates in ocular tissues were at least four times lower than in the human liver homogenate and roughly similar to the activity in rat whole eye sample.

The profile of DME hydrolysis was clearly different from that of NPA in human ocular tissues (Figure 1B). Specific activities were now highest in the retina (~ 2 nmol/min/mg) which showed about two-fold lower or similar activity as compared to the human liver and rat whole eye positive controls, respectively. Moderate activity ($\sim 0.6 \pm 0.1 - 1.2 \pm 0.3$ nmol/min/mg) was seen in the human iris-ciliary body, RPE/choroid, lens and vitreous, while the lowest activities were recorded in conjunctiva and cornea (< 0.2 nmol/min/mg).

FDA hydrolysis rates were again different from the NPA hydrolysis (Figure 1C). The human retina displayed the highest hydrolytic activity at 6.5 ± 1.2 nmol/min/mg which was about two-fold lower than in the human liver but more than four-fold higher than in the rat whole eye homogenate. Iris-ciliary body, vitreous, and RPE/choroid had moderate activities at $2 - 3$ nmol/min/mg, followed by conjunctiva at ~ 1 nmol/min/mg. Activities in the cornea and lens were lower (< 0.5 nmol/min/mg).

20

Procaine has been reported to be a specific substrate for CES2 (Dhananjeyan et al., 2007; Jewell et al., 2007) that can be monitored via the formation of the PABA metabolite. In human ocular tissues, PABA production was observed in all tissues except the lens (Figure 1D). The highest values were seen in the retina (819 ± 211 pmol/min/mg). The activities in RPE/choroid, retina, and vitreous were comparable between 135 ± 56 and 188 ± 12 pmol/min/mg while the cornea and conjunctiva displayed 4- to 8-fold lower activities at 23 ± 11 to 31 ± 12 pmol/min/mg. In contrast, phenacetin hydrolysis by the AADAC to p-phenetidine (Kudo et al., 2000) was below the limit of detection (LLOD) in all ocular tissues except the retina which showed very low activity (0.1 ± 0.04 pmol/min/mg protein). Significant p-phenetidine formation (7.6 ± 0.3 pmol/min/mg protein) was observed in the human liver as excepted (*data not shown*).

Among the human tissues, the retina, iris-ciliary body, and RPE/choroid tended to have the highest specific hydrolytic activities while the cornea and lens contained the lowest activities. When comparing activities among human ocular tissues, the profiles of DME and FDA or procaine hydrolysis rates were more similar to each other ($r^2 = 0.73 - 0.75$) as compared to NPA hydrolysis rates (r^2 0.10 – 0.20), (Supp. Table 4). In addition, hydrolysis rates of FDA and procaine correlated quite well ($r^2 = 0.80$), (Figure 4 and Supp. Fig. 3).

Kinetic parameters

The kinetic parameters were determined in human iris-ciliary and retinal tissues due to their high enzyme activity. For all three substrates NPA, DME, and FDA, the hydrolysis rates largely followed the Michaelis–Menten kinetics as evident from the corresponding Eadie–Hofstee plots (Figure 2) with K_m values of 100 ± 11, 3.0 ± 0.3, and 24 ± 2.1 μM, respectively. The literature K_m values for NPA, DME, and FDA hydrolysis have previously been measured using human liver homogenate (K_m for NPA ∼200 μM; Wang et al., 2011) or liver

21

microsomes (K_m for DME ~5 µM; Hou et al., 2016) and K_m for FDA ~28 µM; Polsky-Fisher et al., 2006). The reported K_m values are fairly similar to the K_m values obtained for FDA and DME and higher for NPA as compared to present experimental conditions.

Inhibition studies

The hydrolytic activities of DME and FDA that are established CES1 and CES2 substrates, respectively, were assessed for inhibition using digitonin (selective for CES1), verapamil, diltiazem, and timolol (selective for CES2) (Figure 3). In human retinal homogenate, digitonin inhibited the DME activity by at least 80% and yielded an IC_{50} value of 27 ± 4.3 µM whereas the extent of inhibition in RPE/choroid was ~62% and the IC_{50} value was 33 ± 9 µM (Figure 3A). These IC_{50} values are well in line with the reported value of 26 ± 3.9 µM that was obtained using recombinant human CES1 (Shimizu et al., 2014). The known CES2 inhibitors verapamil, diltiazem (Figures 3B, 3C) or timolol (*data not shown*) did not inhibit DME activity by more than 15% in either tissue. These findings imply that the CES1 enzyme catalyzes the bulk of DME activity in ocular tissues.

No considerable inhibition of FDA hydrolysis (< 15%) was observed in homogenates of the iris-ciliary body and retina by digitonin (Figure 3D). Verapamil and diltiazem inhibited the FDA hydrolysis moderately by ~50% (Figures 3E, 3F) whereas timolol did not affect the activity (*data not shown*). The reported IC_{50} values for recombinant human CES2 or human liver microsomes were about 5 – 8 µM for verapamil and 4 µM for diltiazem whereas timolol inhibited the reaction very weakly, by 20% at 200 µM (Polsky-Fisher et al., 2006; Yanjiao et al., 2013; Zou et al., 2017). Although these IC_{50} values are smaller than ours, the rank order of inhibitor potency is the same. These data suggest that in addition to CES2, hydrolysis of FDA might also be catalyzed by other esterases.

Quantitative protein expression and correlation with enzyme activities

We report here, for the first time, the comparative expression of esterases in human ocular tissues (Table 2). The positive control sample human liver homogenate displayed high CES1 and CES2 contents, 123 ± 5.0 and 11.5 ± 2.3 pmol/mg protein, respectively, while CES3 content was present at much lower levels (0.5 ± 0.1 pmol/mg protein). These hepatic CES1 protein levels are close to values reported in the literature, indicating that our method was reliable. For example, Wang et al (2016) reported a mean CES1 content of 176 pmol/mg protein in human liver S9 homogenates from 102 individuals (range 42 – 478 pmol/mg). Another study (Sato et al., 2012) found similar CES1 levels at 171 – 801 pmol/mg and CES2 levels at 16.3 – 57.2 pmol/mg using human microsomes. In the other control sample, the rat whole eye homogenate, the CES1 and CES3 contents (1.8 and 2.4 pmol/mg, respectively) were higher than that of CES2 (~0.2 pmol/mg) in line with our earlier data (Hammid et al., 2021).

Among the human ocular tissues, CES1 expression was highest in the iris-ciliary body and retina at 2 – 2.5 pmol/mg protein. Lens, conjunctiva, and RPE/choroid had slightly lower CES1 contents at 1.3 – 1.7 pmol/mg whereas vitreous (0.7 pmol/mg) and cornea (0.2 pmol/mg) displayed significantly lower expression. Contents of other hydrolytic enzymes such as CES2, CES3, and AADAC were undetectable or below the lower limit of quantitation (LLOQ, <0.1 pmol/mg) in all ocular tissues. The membrane marker protein Na^+/K^+ ATPase was also quantified as a reference (Uchida et al., 2013). Na^+/K^+ ATPase was broadly expressed in the retina and RPE/choroid at 5 – 6 pmol/mg, followed by iris-ciliary, conjunctiva, and vitreous at 2 – 4 pmol/mg, while its content was lower in the cornea and lens at 1 and 0.3 pmol/mg, respectively. Human ocular tissues displayed a moderate correlation (r^2

23

= 0.48) between CES1 expression and DME hydrolysis as shown in Figure 4 and Supp. Fig. 3, whereas its correlation with NPA and procaine hydrolysis was low (Supp. Table 4).

Due to the low CES2 levels, we wanted to verify its presence by Western blotting using a CES2 specific antibody. A strong and a weak immunoreactive band at appropriate size (~62 kDa) was observed in human liver and rat whole eye homogenates, respectively (Supp. Fig.1), coinciding with the proteomics results (Table 2). Similarly sized bands were observed in all human ocular tissues except the lens. Small variation in molecular weight around 62 kDa might be due to differentially glycosylated forms of CES2 (Alves et al., 2016). Retina, vitreous, RPE/choroid and rat whole eye displayed an immunoreactive band at 32-33 kDa (Supp. Fig. 1). The higher molecular weight bands might be due to non-specific binding.

Evaluation of posterior tissue contamination

The immunoblot results of posterior tissues with antibodies against the RPE marker bestrophin-1 and the retina marker BDNF are presented in Supp. Fig. 2. A single immunoreactive band at appropriate size of 27-30 kDa for the BDNF precursor (Mowla et al., 2001) was detected in retina but not in vitreous nor RPE/choroid samples. The 64-68 kDa band for bestrophin-1 (Marmorstein et al., 2000) was detectable weakly in the vitreous, moderately in retina and strongest staining was present in the RPE/choroid, indicating some contamination by RPE between these adjacent tissues. However, all esterase activities studied (Figure 1) and CES1 content (Table 2) were highest in retina, lower in RPE/choroid and least in vitreous, suggesting that RPE contamination cannot fully explain the tissue distribution of esterases.

Discussion

This study has, for the first time, quantitated CES isoforms in human ocular tissues using targeted proteomics. We found that CES1 content varies considerably (> 10-fold) among ocular tissues with the highest contents in retina and iris-ciliary body ($\geq$ 2 pmol/mg), and the lowest content in cornea (~ 0.2 pmol/mg). CES2 is detected at much lower content (< 0.1 pmol/mg) in conjunctiva, cornea, retina, and RPE/choroid. Immunochemical analysis confirmed a low expression of the anti-CES2-reactive protein in these tissues. AADAC protein and activity are absent in the ocular samples, matching our findings in rabbits and pigs (Hammid et al., 2021).

Previously, the qualitative detection by proteomics of multiple proteins in human ocular tissues has been reviewed (Ahmad et al., 2018). CES1 was detectable in most ocular tissues including cornea (Galiacy et al., 2011), lens (Hains and Truscott, 2010), RPE/choroid and vitreous (Skeie and Mahajan, 2014; Skeie et al., 2015), and ciliary body and retina (Zhang et al., 2015, 2016) whereas CES2, CES3 or AADAC were not observed. Our quantitative data confirms this ocular profile for CES1 and AADAC, but in contrast, clearly indicates the presence of CES2. Another qualitative study indicated the presence of CES4/CES1P1 while no other CES isoform was identified in the S9 fraction from pooled human whole eyes (Balhara et al., 2021). This sampling approach minimized interindividual variation but diluted

25

the individual tissue contents. Therefore, it is likely that CES1 content was below the detection limit of their method. We did not analyze CES4/CES1P1 which is an inactive truncated 31-kDa enzyme (Uniprot Q9UKY3; Yan et al., 1999). The anti-CES2-reactive band at 32-33 kDa we found in retina, vitreous, and RPE/choroid might explain the presence of CES4 in the whole eye (Balhara et al., 2021). Global RNA expression has recently been determined in multiple ocular tissues by RNA sequencing (Wolf et al., 2022; https://www.eye-transcriptome.com/). The CES1 mRNA has been found at significant levels in conjunctiva, retina, and cornea whereas CES2 mRNA is present ubiquitously. Moderate to strong expression of CES1 and CES2 transcripts has also been reported in the human corneal epithelium tissue (Kaluzhny et al., 2018). Because mRNA and protein expression do not always correlate, these findings do not fully match with our and others' proteomics results but support the presence of CES isoforms in ocular tissues.

The poor availability and small tissue sizes often hinder experimental use of the human eye. Precautions were taken to minimize cross-contamination during surgery and dissection, and posterior tissues were evaluated by Western blotting. We found BDNF only in the retina, verifying the clean separation of retina from RPE. The RPE marker bestrophin-1 was present in descending order RPE/choroid, retina and vitreous, suggesting some leakage of RPE tissue into these adjacent tissues. However, the esterase activities and CES1 content did not follow the same pattern as bestrophin-1 because the former values were higher in retina than in RPE/choroid or vitreous. Thus, presence of esterases cannot be explained by significant contamination. Because the samples came from diseased persons, tissue damage prior to dissection cannot be excluded. Both human and mouse proteomic studies (Skeie et al., 2015; Mirzaei et al., 2017; Zhang et al., 2015; Zhao et al., 2018) suggest that the vitreous contains proteins originating from the retina and RPE. Moreover, RNA expression studies (Wolf et al.,

2022) show that bestrophin-1 mRNA is present in central retina and RPE/choroid in equal levels.

The contamination problem may confound any RNA and proteomics expression studies. The available reports have used similar dissection techniques, but they have not evaluated the extent of contamination by e.g. immunochemistry. One possibility to avoid contamination and elucidate cell-specific expression is in situ hybridization with probes specific for CES isoform mRNAs. This technique is only semi-quantitative and would not inform about cellular protein or activity levels. Immunohistochemistry of ocular cell types are likely confounded by e.g., inadequate specificity of the antibodies and tissue autofluorescence, especially when probing for less abundant enzymes. Even though cell type-specific CES expression would be valuable, we focused on CES expression at the average tissue level which is sufficient for pharmacokinetic modeling.

Another limitation of our study is that our findings were generated mainly using ocular tissues from elderly glaucoma patient donors or post-mortem patients. Only one patient was a teenager. While it is established that hepatic drug-metabolizing enzymes mature quite early during development (e.g., van Groen et al., 2021), we have no evidence on whether levels of ocular CES enzymes are similar in younger patients or in healthy persons.

This is a first comprehensive study of esterase-mediated activities in seven human eye tissues. The highest NPA hydrolysis rates were in the iris-ciliary body and vitreous whereas cornea, conjunctiva, retina, and RPE/choroid showed similar activities, and lens displayed the lowest rates. For DME, the activities were in the descending order of retina > iris-ciliary body and RPE/choroid > vitreous and lens > conjunctiva and cornea. For FDA, the hydrolysis rates

were highest in retina and iris-ciliary body and lowest in cornea and lens. These distinct profiles imply dissimilar tissue expression of esterases.

Our studies utilized selective substrates and inhibitors established for the human CES1 and CES2 enzymes. Based on good correlation between hydrolysis rates and enzyme contents, DME appears a specific CES1 substrate, which is supported by efficient inhibition of DME hydrolysis by digitonin. FDA seems to be less specific as a CES2 substrate because its hydrolysis was inhibited maximally 50% by verapamil and diltiazem, indicating that other esterases capable of hydrolyzing FDA are present in retina and iris-ciliary body. Although CES1 can metabolize FDA (but with 46-fold lower V_{max} than CES2; Wang et al., 2011), digitonin did not inhibit this reaction. FDA can be hydrolyzed by AADAC (Fukami et al., 2015) which seems absent in ocular tissues. Candidate esterases might include paraoxonases, lipases or aryl esterases qualitatively present in ocular tissues (Ahmad et al., 2018) but their preference for FDA as a substrate is unknown. More careful analysis of tissues with low enzymatic activities and in-depth analysis of ocular esterase activities are thus warranted.

Previously, we measured the corresponding CES isoforms and activities in rabbit and pig ocular tissues (Hammid et al., 2021). Among the matching tissues sampled, NPA hydrolysis in human conjunctiva and retina were similar (21 – 32 nmol/min/mg) while human cornea showed 1.3- and 2.7-fold lower and vitreous displayed 1.8- and 3.3-fold higher values compared to the rabbit and pig tissues, respectively. For DME, the differences were more pronounced: human cornea and conjunctiva had 6- to 20-fold lower activities while the activity was up to 20-fold higher than in rabbit and pig retinal homogenates. For FDA and procaine, human conjunctiva and cornea had 1.3- to 10-fold lower activities than in rabbit tissues whereas human retina displayed 8- to 10-fold higher values than rabbit retina. FDA

and procaine hydrolysis in pig tissues were generally lower and relatively constant (< 0.1 nmol/min/mg) (Hammid et al., 2021). Even though human RPE and choroid were not analyzed separately, higher esterase activities in animal choroids suggest that the human choroid may contain more activity than the RPE. Finally, expression of CES1 appears higher in conjunctiva, vitreous, retina and RPE/choroid compared to the same rabbit tissues while CES2 levels were roughly similar although low. Pig has a very strong corneal expression of CES1 (~8 pmol/mg) compared to the other species (0.14 – 0.2 pmol/mg) (Hammid et al., 2021). These findings indicate significant species differences in ocular tissue-specific expression of CES isoforms.

Rabbit is considered the most relevant model to translate preclinical results of ocular drug candidates to humans (Del Amo and Urtti, 2015; del Amo et al., 2017). Previously, we noted a rapid hydrolysis of cefuroxime axetil after intravitreal and intracameral injections into rabbit eyes (del Amo et al., 2022). With the intracameral route, the main hydrolytic sites were the cornea, iris-ciliary body, and aqueous humor. With the intravitreal injection, retina, vitreous and iris-ciliary body seemed the most active tissues. Considering the comparatively greater human CES1 contents in conjunctiva, vitreous, retina, and RPE/choroid and its high expression in the human iris-ciliary body, the contribution of cornea for prodrug hydrolysis may be overestimated if based solely on rabbit *in vivo* studies. Cornea may exhibit "first-pass metabolism" for drugs applied topically but acting in other ocular locations. Thus, the relative role of tissue hydrolysis depends on the administration route. Similar species differences that may complicate translational studies have been observed (e.g., Coupland et al., 1994; Burkina et al., 2016; Cirello et al., 2017; Heikkinen et al., 2018). Therefore, studies on expression and catalytic profiles of drug-metabolizing enzymes in preclinical species are necessary.

In conclusion, this study has generated novel data on CES activities and quantities in seven different human ocular tissues. Combined with detailed information from preclinical species

(Hammid et al., 2021), it provides a deeper insight into ocular drug metabolism and accelerates the process of ocular drug development, as the human ocular metabolic data and interspecies comparisons are useful for the design of pharmacokinetic and pharmacodynamic studies on therapeutics.

Authorship Contributions

Participated in research design: **Anam Hammid, Paavo Honkakoski.**

Conducted experiments: **Anam Hammid, John K. Fallon, Toni Lassila.**

Samples collection and dissection: **Paula Vieiro, Francisco Gonzalez, Anam Hammid, Anusha Balla**.

Performed data analysis: **Anam Hammid, John K. Fallon, Toni Lassila**.

Wrote the original manuscript: **Anam Hammid**

Writing – review & editing: **Paavo Honkakoski, Anam Hammid, John K. Fallon, Arto Urtti, Toni Lassila, Philip C. Smith, Ari Tolonen, Francisco Gonzalez.**

References

Ahmad MT, Zhang P, Dufresne C, Ferrucci L, and Semba RD (2018) The human eye proteome project: updates on an emerging proteome. *Proteomics* **18**:5-6

Al-Ghananeem AM, and Crooks PA (2007) Phase I and phase II ocular metabolic activities and the role of metabolism in ophthalmic prodrug and codrug design and delivery. *Molecules* **12**:373–388.

Alves M, Lamego J, Bandeiras T, Castro R, Tomás H, Coroadinha AS, Costa J, and Simplício AL (2016) Human carboxylesterase 2: Studies on the role of glycosylation for enzymatic activity. *Biochemistry and Biophysics Reports* **5**:105–110.

Argikar UA, Dumouchel JL, Dunne CE, and Bushee AJ (2017) Ocular non-P450 oxidative, reductive, hydrolytic, and conjugative drug metabolizing enzymes. *Drug Metabolism Reviews* **49**:372–394.

Argikar UA, Dumouchel JL, Dunne CE, Saran C, Cirello AL, and Gunduz M (2016) Ocular metabolism of levobunolol: Historic and emerging metabolic pathways. *Drug Metabolism and Disposition* **44**:1304–1312.

Attar M, Shen J, Ling K-HJ, and Tang-Liu D (2005) Ophthalmic drug delivery considerations at the cellular level: drug-metabolising enzymes and transporters. *Expert Opinion on Drug Delivery* **2**:891–908.

Balhara A, Basit A, Argikar UA, Dumouchel JL, Singh S, and Prasad B (2021) Comparative proteomics analysis of the postmitochondrial supernatant fraction of human lens-free whole eye and liver. *Drug Metabolism and Disposition* **49**:592-600

Balla A, Auriola S, Grey AC, Demarais NJ, Valtari A, Heikkinen EM, Toropainen E, Urtti A, Vellonen KS, and Ruponen M (2021) Partitioning and spatial distribution of drugs in ocular surface tissues. *Pharmaceutics* **13**:1–15.

Bradford MM (1976) A rapid and sensitive method for the quantitation of microgram quantities of protein utilizing the principle of protein-dye binding. *Analytical Biochemistry* **72**:248–254.

Burkina V, Rasmussen MK, Pilipenko N, and Zamaratskaia G (2016) Comparison of xenobiotic-metabolising human, porcine, rodent, and piscine cytochrome P450. *Toxicology* **375**:10–27.

Bushee JL, Dunne CE, and Argikar UA (2015) An in vitro approach to investigate ocular metabolism of a topical, selective β1-adrenergic blocking agent, betaxolol. *Xenobiotica* **45**:396–405.

Cirello AL, Dumouchel JL, Gunduz M, Dunne CE, and Argikar UA (2017) In vitro ocular metabolism and bioactivation of ketoconazole in rat, rabbit and human. *Drug Metabolism and Pharmacokinetics* **32**:121–126.

Coupland SE, Penfold PL, and Billson FA (1994) Hydrolases of anterior segment tissues in the normal human, pig and rat eye: a comparative study. *Graefe's Archive for Clinical and Experimental Ophthalmology* **232**:182–191.

Davies SS, Ju WK, Neufeld AH, Abran D, Chemtob S, and Roberts LJ (2003) Hydrolysis of bimatoprost (Lumigan) to its free acid by ocular tissue in vitro. *Journal of Ocular Pharmacology and Therapeutics* **19**:45–54.

del Amo EM, Hammid A, Tausch M, Toropainen E, Sadeghi A, Valtari A, Puranen J,

Reinisalo M, Ruponen M, Urtti A, Sauer A, and Honkakoski P (2022) Ocular metabolism and distribution of drugs in the rabbit eye: Quantitative assessment after intracameral and intravitreal administrations. *International Journal of Pharmaceutics* **613:** 121361.

del Amo EM, Rimpelä A-KK, Heikkinen E, Kari OK, Ramsay E, Lajunen T, Schmitt M, Pelkonen L, Bhattacharya M, Richardson D, Subrizi A, Turunen T, Reinisalo M, Itkonen J, Toropainen E, Casteleijn M, Kidron H, Antopolsky M, Vellonen KS, Ruponen M, and Urtti A (2017) Pharmacokinetic aspects of retinal drug delivery. *Progress in Retinal and Eye Research* **57**:134–185.

Del Amo EM, and Urtti A (2015) Rabbit as an animal model for intravitreal pharmacokinetics: Clinical predictability and quality of the published data. *Experimental Eye Research* **137**:111–124.

Dhananjeyan MR, Bykowski C, Trendel JA, Sarver JG, Ando H, and Erhardt PW (2007) Simultaneous determination of procaine and para-aminobenzoic acid by LC-MS/MS method. *Journal of Chromatography B: Analytical Technologies in the Biomedical and Life Sciences* **847**:224–230.

Dumouchel JL, Chemuturi N, Milton MN, Camenisch G, Chastain J, Walles M, Sasseville V, Gunduz M, Iyer GR, and Argikar UA (2018) Models and approaches describing the metabolism, transport, and toxicity of drugs administered by the ocular route. *Drug Metabolism and Disposition* **46**:1670–1683.

Duvvuri S, Majumdar S, and Mitra AK (2004) Role of metabolism in ocular drug delivery. *Current Drug Metabolism* **5**:507–15.

Ellis PP, Littlejohn K, and Deitrich RA (1972) Enzymatic hydrolysis of pilocarpine. *Investigative Ophthalmology* **11**:747–751.

Fukami T, Kariya M, Kurokawa T, Iida A, Nakajima M (2015) Comparison of substrate specificity among human arylacetamide deacetylase and carboxylesterases. *European Journal of Pharmaceutical Sciences* **78**:47-53.

Galiacy SD, Froment C, Mouton-Barbosa E, Erraud A, Chaoui K, Desjardins L, Monsarrat B, Malecaze F, and Burlet-Schiltz O (2011) Deeper in the human cornea proteome using nanoLC-Orbitrap MS/MS: An improvement for future studies on cornea homeostasis and pathophysiology. *Journal of Proteomics* **75**:81–92.

Hains PG, and Truscott RJW (2010) Age-dependent deamidation of lifelong proteins in the human lens. *Investigative Ophthalmology and Visual Science* **51**:3107–3114.

Hammid A, Fallon JK, Lassila T, Salluce G, Smith PC, Tolonen A, Sauer A, Urtti A, and Honkakoski P (2021) Carboxylesterase activities and protein expression in rabbit and pig ocular tissues. *Molecular Pharmaceutics* **18**:1305–1316.

Heikkinen EM, del Amo EM, Ranta VP, Urtti A, Vellonen KS, and Ruponen M (2018) Esterase activity in porcine and albino rabbit ocular tissues. *European Journal of Pharmaceutical Sciences* **123**:106–110.

Hellberg MR, Ke T-L, Haggard K, Klimko PG, Dean TR, and Graff G (2003) The hydrolysis of the prostaglandin analog prodrug bimatoprost to 17-phenyl-trinor PGF2 α by human and rabbit ocular tissue. *Journal of Ocular Pharmacology and Therapeutics* **19**: 97-103.

Hou J, Yang L, Lei W, Cheng H-L, Jin Q, Wang D-D, Zou L-W, Lv X, and Ge G-B (2016) A bioluminescent sensor for highly selective and sensitive detection of human

carboxylesterase 1 in complex biological samples. *Chemical Communications* **52**:3183–3186.

Jewell C, Ackermann C, Payne NA, Fate G, Voorman R, Williams FM, and Al JET (2007) Specificity of procaine and ester hydrolysis by human, minipig, and rat skin and liver. *Drug Metabolism and Disposition* **35**:2015–2022.

Kaluzhny Y, Kinuthia MW, Truong T, Lapointe AM, Hayden P, and Klausner M (2018) New human organotypic corneal tissue model for ophthalmic drug delivery studies. *Investigative Ophthalmology and Visual Science* **59**:2880–2898.

Khatri R, Fallon JK, Rementer RJB, Kulick NT, Lee CR, and Smith PC (2019) Targeted quantitative proteomic analysis of drug metabolizing enzymes and transporters by nano LC-MS/MS in the sandwich cultured human hepatocyte model. *Journal of Pharmacological and Toxicological Methods* **98**:106590.

Kudo S, Umehara KEN, Hosokawa M, Miyamoto G, Chiba K and Satoh T (2000) Phenacetin deacetylase activity in human liver microsomes: distribution, kinetics, and chemical inhibition and stimulation. *The Journal of Pharmacology and Experimental Therapeutics* **294**:80–8.

Lassila T, Rousu T, Mattila S, Chesné C, Pelkonen O, Turpeinen M, and Tolonen A (2015) Formation of GSH-trapped reactive metabolites in human liver microsomes, S9 fraction, HepaRG-cells, and human hepatocytes. *Journal of Pharmaceutical and Biomedical analysis* **115**:345–351.

Lee VHL, Morimoto KW, and Stratford RE (1982) Esterase distribution in the rabbit cornea and its implications in ocular drug bioavailability. *Biopharmaceutics & Drug*

Disposition **3**:291–300.

Lee VHL (1983) Esterase activities in adult rabbit eyes. *Journal of Pharmaceutical Sciences* **72**:239–244.

Lee VHL, Stratford RE, and Morimoto KW (1983) Age-related changes in esterase activity in rabbit eyes. *International Journal of Pharmaceutics* **13**:183–195.

Li AP (2021) Drug-metabolism enzymes and transporter activities as risk factors of selected marketed drugs associated with drug-induced fatalities. *Transporters and Drug-Metabolizing Enzymes in Drug Toxicity* 41–77, John Wiley & Sons, Inc.

Macha S, Duvvuri S, and Mitra AK (2004) Ocular disposition of novel lipophilic diester prodrugs of ganciclovir following intravitreal administration using microdialysis. *Current Eye Research* **28**:77–84.

Mandell AI, Stentz F, and Kitabchi AE (1978) Dipivalyl Epinephrine: A new pro-drug in the treatment of glaucoma. *Ophthalmology* **85**:268–275.

Marmorstein AD, Marmorstein LY, Rayborn M, Wang X, Hollyfield JG, and Petrukhin K (2000) Bestrophin, the product of the Best vitelliform macular dystrophy gene (VMD2), localizes to the basolateral plasma membrane of the retinal pigment epithelium. *Proceedings of the National Academy of Sciences* **97**:12758-12763.

Mowla SJ, Farhadi HF, Pareek S, Atwal JK, Morris SJ, Seidah NG, and Murphy RA (2001) Biosynthesis and post-translational processing of the precursor to brain-derived neurotrophic factor. *Journal of Biological Chemistry* **276**:12660-12666.

Mirzaei M, Gupta VB, Chick JM, Greco TM, Wu Y, Chitranshi N, Wall RV, Hone E, Deng

L, Dheer Y, Abbasi M, Rezaeian M, Braidy N, You Y, Salekdeh GH , Haynes PA, Molloy MP, Martins R, Cristea IM, Gygi SP Graham SL and Gupta, V. K. (2017) Age-related neurodegenerative disease associated pathways identified in retinal and vitreous proteome from human glaucoma eyes. *Scientific Reports* **7**: 1-16

Nakamura M, Shirasawa E, and Hikida M (1993) Characterization of esterases involved in the hydrolysis of dipivefrin hydrochloride. *Ophthalmic Research* **25**:46–51.

Polsky-Fisher SL, Cao H, Lu P, and Gibson CR (2006) Effect of cytochromes P450 chemical inhibitors and monoclonal antibodies on human liver microsomal esterase activity. *Drug Metabolism and Disposition* **34**:1361–1366.

Saarinen-Savolainen P, Järvinen T, Suhonen P, and Urtti A (1996) Amphiphilic properties of pilocarpine prodrugs. *International Journal of Pharmaceutics* **133**:171–178.

Sato Y, Miyashita A, Iwatsubo T, and Usui T (2012) Simultaneous absolute protein quantification of carboxylesterases 1 and 2 in human liver tissue fractions using liquid chromatography-tandem mass spectrometry. *Drug Metabolism and Disposition* **40**:1389–1396.

Shimizu M, Fukami T, Nakajima M, and Yokoi T (2014) Screening of specific inhibitors for human carboxylesterases or arylacetamide deacetylase. *Drug Metabolism and Disposition* **42**:1103–1109.

Sjöquist B, Basu S, Byding P, Bergh K, and Stjernschantz J (1998) The pharmacokinetics of a new antiglaucoma drug, latanoprost, in the rabbit. *Drug Metabolism and Disposition* **26**:745–754.

Skeie JM, and Mahajan VB (2014) Proteomic landscape of the human choroid-retinal

pigment epithelial complex. *JAMA Ophthalmology* **132**:1271–1281.

Skeie JM, Roybal CN, and Mahajan VB (2015) Proteomic insight into the molecular function of the vitreous. *PLoS ONE* **10**: e0127567.

Uchida Y, Tachikawa M, Obuchi W, Hoshi Y, Tomioka Y, Ohtsuki S, and Terasaki T (2013) A study protocol for quantitative targeted absolute proteomics (QTAP) by LC-MS/MS: application for inter-strain differences in protein expression levels of transporters, receptors, claudin-5, and marker proteins at the blood–brain barrier in ddY, FVB, and C57BL/6J mice. *Fluids and Barriers of the CNS* **10**:1-22.

Van Groen BD, Nicolaï J, Kuik AC, Van Cruchten S, Van Peer E, Smits A, Schmidt S, de Wildt SN, Allegaert K, De Schaepdrijver L, Annaert P and Badée J (2021) Ontogeny of hepatic transporters and drug-metabolizing enzymes in humans and in nonclinical species. *Pharmacological Reviews* **73**:597-678.

Volotinen M, Hakkola J, Pelkonen O, Vapaatalo H, and Mäenpää J (2011) Metabolism of ophthalmic timolol: New Aspects of an Old Drug. *Basic and Clinical Pharmacology and Toxicology* **108**:297–303.

Wang J, Williams ET, Bourgea J, Wong YN, Patten CJ, Al WET, Wang J, Williams ET, Bourgea J, Wong YN, and Patten CJ (2011) Characterization of recombinant human carboxylesterases: fluorescein diacetate as a probe substrate for human carboxylesterase 2. *Drug Metabolism and Disposition* **39**:1329–1333.

Wang X, Liang Y, Liu L, Shi J, and Zhu H (2016) Targeted absolute quantitative proteomics with SILAC internal standards and unlabeled full-length protein calibrators (TAQSI). *Rapid Communications in Mass Spectrometry* **30**:553–561.

Watanabe A, Fukami T, Takahashi S, Kobayashi Y, Nakagawa N, Nakajima M, and Yokoi T (2010) Arylacetamide deacetylase is a determinant enzyme for the difference in hydrolase activities of phenacetin and acetaminophen. *Drug Metabolism and Disposition* **38**:1532–1537.

Wolf J, Boneva S, Schlecht A, Lapp T, Auw-Haedrich C, Lagrèze W, Agostini H, Reinhard T, Schlunck G, and Lange C (2022) The Human Eye Transcriptome Atlas: A searchable comparative transcriptome database for healthy and diseased human eye tissue. *Genomics* **114**:110286.

Xiang CD, Batugo M, Gale DC, Zhang T, Ye J, Li C, Zhou S, Wu EY, and Zhang EY (2009) Characterization of human corneal epithelial cell model as a surrogate for corneal permeability assessment: metabolism and transport. *Drug Metabolism and Disposition* **37**:992–998.

Yan B, Matoney L, and Yang D (1999) Human carboxylesterases in term placentae: enzymatic characterization, molecular cloning and evidence for the existence of multiple forms. *Placenta* **20:** 599-607.

Yanjiao X, Chengliang Z, Xiping L, Tao W, Xiuhua R, and Dong L (2013) Evaluation of the inhibitory effects of antihypertensive drugs on human carboxylesterase in vitro. *Drug Metabolism and Pharmacokinetics* **28**:468–474.

Zhang P, Dufresne C, Turner R, Ferri S, Venkatraman V, Karani R, Lutty GA, Van Eyk JE, and Semba RD (2015) The proteome of human retina. *Proteomics* **15**:836–840.

Zhang P, Kirby D, Dufresne C, Chen Y, Turner R, Ferri S, Edward DP, Van Eyk JE, and Semba RD (2016) Defining the proteome of human iris, ciliary body, retinal pigment

epithelium, and choroid. *Proteomics* **16**:1146–1153.

Zhang Z, and Tang W (2018) Drug metabolism in drug discovery and development. *Acta Pharmaceutica Sinica B* **8**:721–732.

Zhao Y, Weber SR, Lease J, Russo M, Siedlecki CA, Xu LC, Chen H, Wang WW, Ford M, Simó R and Sundstrom, JM (2018) Liquid biopsy of vitreous reveals an abundant vesicle population consistent with the size and morphology of exosomes. *Translational Vision Science & Technology* **7**: 6-6.

Zou LW, Jin Q, Wang DD, Qian QK, Hao DC, Ge GB, and Yang L (2017) Carboxylesterase inhibitors: an update. *Current Medicinal Chemistry* **25**:1627–1649.

Figure legends

Figure 1

Esterase activities in human ocular tissues. Hydrolysis of 4-nitrophenol acetate (NPA, panel A), D-luciferin methyl ester (DME, panel B), fluorescein diacetate (FDA, panel C), and procaine (panel D) in human ocular tissue samples and positive controls (rat whole eye and human liver homogenates). The data shown are means ± SD from three separate tissue pools while individual tissue pool is represented by a dot. Each pool was measured using three technical assay replicates. Statistical comparison between the tissues was done by the Mann–Whitney nonparametric test and significant differences to the tissue with the highest activity (A: iris-ciliary body, B - D: retina) are indicated as follows: *, $p < 0.05$, **, $p < 0.01$, ***$p < 0.001$.

Figure 2

Michaelis-Menten kinetics of NPA, DME, and FDA hydrolysis. The substrate concentration ranges of 4-nitrophenol acetate (NPA) 37.5 – 2000 µM (A), D-luciferin methyl ester (DME) 0.3 – 20 µM (B) and fluorescein diacetate (FDA) 3.12 – 200 µM (C) were used to measure the reaction rates with the iris-ciliary body (**A**) or retina (**B**, **C**) homogenates as enzyme sources. Each data point corresponds to the mean ± SD of three replicates. The non-linear regression in GraphPad Prism was used to calculate the apparent maximum velocity, V_{max} and Michaelis constant, K_m values. The insets show the Eadie-Hofstee plots of the primary data. The slightly convex Eadie-Hofstee plots in panels **A** and **B** suggested possible

substrate inhibition which was also assessed. The corresponding inhibition constant, Ki estimates were 7.5 ± 2.4 mM (**A**) and 35 ± 13 µM (**B**), respectively.

Figure 3

Inhibition of DME and FDA hydrolysis. Inhibition of D-luciferin methyl ester (DME **, A** – C) and fluorescein diacetate (FDA, **D** – **F**) hydrolysis by the CES1-selective inhibitor digitonin (**A**, **D**) and CES2-selective inhibitors verapamil (**B**, **E**) and diltiazem (**C**, **F**) were conducted at 5 µM DME and 30 µM FDA with increasing inhibitor concentrations (digitonin, verapamil, 3 – 200 µM; diltiazem 0.13-100 µM) using the human RPE/choroid, iris-ciliary body, and retina homogenates as indicated. The maximal inhibitory concentration, IC_{50} values were calculated using non-linear regression analysis with GraphPad Prism. Each data point represents the mean $\pm$ SD of three replicates.

Figure 4

Correlation between the human CES1 content and hydrolysis activities. Pearson correlation coefficients between the CES1 content and DME hydrolysis (**A**) and between fluorescein diacetate (FDA) and procaine hydrolysis (**B**) in human ocular tissues are shown. The horizontal bars displayed in Figures A and B represent the standard deviations in CES1 content and FDA hydrolysis activity, respectively, in ocular tissues. The vertical bars show the standard deviations in DME (A) and procaine (B) hydrolysis in ocular tissues.

Table 1. List of peptides used for proteomic quantification of human ocular tissues and rat and human control samples

Enzyme	Peptides sequences	Species (UniProt ID)
CES1	FWANFA**R***[505,503]	human (P23141), rat (Q63108)
CES2	ADHGDELPFVF**R***[466]	human (O00748)
	AGVHTFLGIPFA**K***[67]	rat (A0A0G2K455)
CES3	LAFPEATEEE**K**[490]	human (Q6UWW8)
	NTIYPLTVDGTVFP**K***[323]	
	TPEEILAE**K***[338]	rat (P16303)
	FAPPQPAEPWNFVK[78]	
AADAC	FWSEYFTTD**R***[258]	human (P22760), rat (Q9QZH8)
	YPGFLDV**R**[318, 257]	human (P22760)
	TPTPGSLELAQ**K***[309]	rat (Q9QZH8)
Na⁺/K⁺ ATPase	AAVPDAVG**K***	both species

K/R shows the ^{13}C and ^{15}N isotope-labeled residues. The C-terminal residue number in the respective protein is indicated for each species. SpikeTides^{TM}_TQL peptides were used as internal standard quantifiers. The concentration of each peptide in the initial cocktail was 20 nM. The peptide mix was dissolved in a solution of 0.1 M ammonium bicarbonate:ACN (1:4) and used for the MRM quantitation. Peptides marked with an asterisk (*) were used to report protein concentration, and the others were used to confirm the presence of the target protein.

Table 2. Contents of hydrolytic enzymes in human ocular tissue homogenates.

Protein	Standard PEPTIDE	OCULAR TISSUES (PMOL/MG)							CONTROL SAMPLES (PMOL/MG)	
		Conjunctiva	Cornea	Vitreous	Lens	Iris-ciliary body	Retina	RPE/ choroid	Human liver	Rat eye
CES1	FWANFAR	1.4 ± 0.2	0.2 ± 0.1	0.7 ± 0.2	1.7 ± 0.4	2.6 ± 0.6	2.0 ± 0.6	1.3 ± 0.1	123.4 ± 5.0	1.8 ± 0.1
CES2	ADHGDELPFVFR	< 0.1	< 0.1	<LLOD	<LLOD	<LLOD	< 0.1	< 0.1	11.5 ± 2.3	0.2 ± 0.1
CES3	NTIYPLTVDGTVFPK	<LLOD	<LLOD	<LLOD	<LLOD	<LLOD	<LLOD	<LLOD	0.5 ± 0.1	2.4 ± 0.5
AADAC	FWSEYFTTDR	<LLOD	<LLOD	<LLOD	<LLOD	<LLOD	<LLOD	<LLOD	2.8 ± 0.2	0.2 ± 0.1
NA$^+$/K$^+$ ATPASE	AAVPDAVGK	3.0 ± 0.7	1.0 ± 0.5	2.0 ± 0.7	0.3 ± 0.1	3.6 ± 1.6	6.0 ± 1.3	5.1 ± 2.4	1.4 ± 0.1	2.5 ± 0.6

* LLOQ = 0.1 pmol/mg; LLOD = 3 × signal/noise ration ~0.02 pmol/mg.
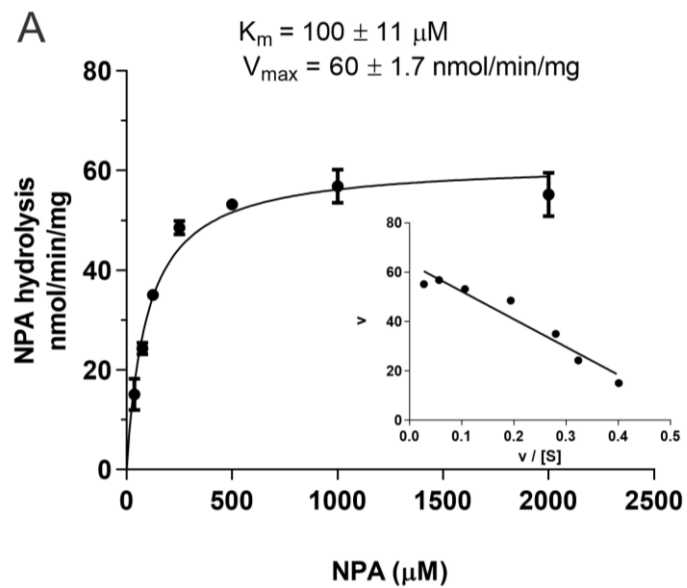
46

Figure 1

Figure 2

A

$K_m = 100 \pm 11 \; \mu M$
$V_{max} = 60 \pm 1.7 \; nmol/min/mg$

B

$K_m = 3.0 \pm 0.3 \; \mu M$
$V_{max} = 0.7 \pm 0.1 \; nmol/min/mg$

C

$K_m = 24 \pm 2.1 \; \mu M$
$V_{max} = 1.0 \pm 0.1 \; nmol/min/mg$

Figure 3

Figure 4